Environmental Science
Water Research & Technology

Bacteria Poration on Modified Boron-Doped Diamond Electrode Surfaces Induced by Divalent Cation Chelation

Journal:	*Environmental Science: Water Research & Technology*
Manuscript ID	EW-ART-12-2019-001108.R2
Article Type:	Paper

Water Impact Statement

Biofouling of surfaces is a wide-spread problem in water treatment, which has performance and health risks. This work showed that modifying electrodes with specific functional groups could induce bacteria poration via chelation of divalent cations from their outer membrane, which suggests it may be a viable method to prevent biofouling of electrode surfaces that are operated at low applied potentials.

Bacteria Poration on Modified Boron-Doped Diamond Electrode Surfaces Induced by Divalent Cation Chelation

Meng-Hsuan Lin[§], Shafigh Mehraeen[§], Gang Cheng[§], Cory Rusinek[†], and Brian P. Chaplin[§*]

[§]Department of Chemical Engineering, University of Illinois at Chicago, 945 W. Taylor St., Chicago, IL 60608

[†]MSU-Fraunhofer Center for Coatings and Diamond Technologies, 1449 Engineering Research Ct., East Lansing, MI 48824

*Corresponding author at: Department of Chemical Engineering, University of Illinois at Chicago, Chicago, IL 60607, USA

E-mail address: chaplin@uic.edu (Brian P. Chaplin)

Phone No.: +13129960288

TOC Entry

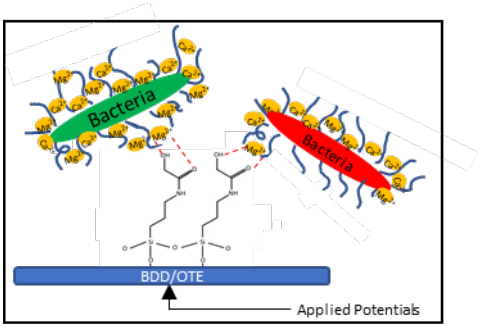

This work showed that divalent ions from the outer membrane of bacteria can be chelated by N-propyl-2-hydroxyacetamide functional groups that were immobilized on boron-doped diamond electrodes.

Abstract

This research investigated mechanisms for biofouling control at modified boron-doped diamond (BDD) electrode surfaces polarized at low applied potentials (e.g., -0.2 to 1 V versus Ag/AgCl), using *Pseudomonas aeruginosa* (PAO1) as a model pathogenic organism. Results indicated that electrostatic interactions and electrochemical reactions under polarized conditions can affect cell attachment and poration, respectively. However, results suggested that divalent ions from the outer membrane of PAO1 can be chelated by N-propyl-2-hydroxyacetamide functional groups that were immobilized on a BDD optically transparent electrode (termed OH-BDD/OTE). It was observed that two- to three-fold higher percentage of porated bacteria were observed on the OH-BDD/OTE compared with BDD/OTE under applied anodic potentials between 0.1 to 0.5 V vs Ag/AgCl. Density functional theory calculations indicated that the chelation mechanism was thermodynamically favorable. Zeta potential measurements of the PAO1 bacteria as a function of chelator and Mg^{2+} concentrations were performed and interpreted using a mathematical model based on the nonlinear Poisson-Boltzmann equation. Results supported the chelation mechanism for bacteria poration, which indicates that electrode modification may be a viable method to prevent biofouling of electrode surfaces that are operated at low applied potentials.

Keywords: Electrochemical disinfection, chelation, finite difference method, nonlinear Poisson-Boltzmann equation

Introduction

The interaction between microorganisms and surfaces has become a focal point of scientific investigations in both natural and engineered settings. Bacteria can often have negative impacts in several industries, such as water treatment and distribution,[1] food,[2,3] and medical device implants.[4,5] These industries spend significant time and resources to combat the growth of biofilms on pipes, heat exchangers, membranes, medical tools and implants, and other surfaces.[6–8] As a result, it is important to understand methods and mechanisms that control bacteria attachment and cause inactivation.

Electrochemical techniques have emerged as potentially effective biofouling control strategies.[9–14] However, high cell potentials (e.g., > 5.0 V) are often needed to generate sufficient disinfectant concentrations.[15] Therefore, electrochemical techniques are not always cost effective due to high power consumption, and other electrochemical water treatment methods, such as capacitive deionization,[16,17] experience biofouling due to their low operating cell potentials (e.g., ~ 1.0 V). Recent work has shown that reactive oxygen species (ROS) and Cl-based oxidants can be generated at electrode surfaces at low-applied potentials (≤ |1.0|V vs. Ag/AgCl), and can cause poration of bacterial cell membranes.[18] However, there is still a need to develop strategies that increase antimicrobial activity of electrode surfaces at low cell potentials for effective biofouling control.

Several studies have shown that chelators such as citrate, phosphate, ethylene-bis(oxyethylenenitrilo)tetraacetic acid (EGTA), ethylenediaminetetraacetic acid (EDTA), and hexametaphosphate possess antibacterial activity.[19–21] These chelators extract Mg^{2+}, Ca^{2+} and other divalent ions from the lipopolysaccharides (LPS) of the cell membrane, which causes membrane destabilization.[22,23] Studies have shown that chelators can be immobilized on surfaces to impart

antimicrobial activity. For example, EDTA was used to inactivate *P. aeruginosa* amd *Salmonella enterica serovar* bacteria by chelating Mg^{2+}, Ca^{2+}, and Fe^{2+} from their cell membranes.[19,24] In addition, polyphosphate has also been shown to chelate divalent cations from the cell membrane of *Bacillus cereus,* which caused growth inhibition and cell lysis.[25] Chelator coatings on electrodes have been studied and applied for biosensing purposes[26–28] and as electrocatalysts.[29] However, to our knowledge this strategy has not been tested on electrode surfaces for antimicrobial control during water treatment.

In this study we investigated the attachment and antimicrobial properties of functionalized electrode surfaces under low applied potentials between -0.2 and 1.0 V vs Ag/AgCl. BDD electrodes were used as model stable electrode surfaces and modified with N-propyl-2-hydroxyacetamide groups to produce distinct chelation sites. These modified electrodes were tested for their antibacterial activity using *Pseudomonas aeruginosa* (POA1) as a model biofilm forming bacteria, which is a known opportunistic pathogen that causes severe acute and chronic infections within the urinary and respiratory tracts of humans.[30] The electrode surfaces were characterized by cyclic voltammetry (CV) and X- ray photoelectron spectroscopy (XPS), and POA1 attachment and poration studies were conducted as a function of the applied potential and Mg^{2+} concentration. Experimental results suggested that the N-propyl-2-hydroxyacetamide groups acted as divalent chelation sites that caused bacteria poration, which were supported by density functional theory (DFT) calculations. Zeta potential measurements of the PAO1 bacteria as a function of chelator and Mg^{2+} concentrations were performed and interpreted using a mathematical model based on the nonlinear Poisson-Boltzmann equation. These results supported the chelation mechanism for bacteria poration.

Materials and Methods

83 ***Reagents.*** Sodium perchlorate ($NaClO_4$), phosphate buffer saline (PBS, with a composition of:
84 pH = 7.4, 137 mM NaCl, 2.7 mM KCl, 10 mM Na_2HPO_4 and 1.8 mM KH_2PO_4), glycolic acid
85 (GA), magnesium chloride hexahydrate ($MgCl_2{\cdot}6H_2O$), potassium hexacyanoferrate (III)
86 ($K_3[Fe(CN)_6]$), potassium hexacyanoferrate (II) ($K_4[Fe(CN)_6]$), hexaamineruthenium (II) chloride
87 ($Ru(NH_3)_6Cl_2$), hexaamineruthenium (III) chloride ($Ru(NH_3)_6Cl_3$), glycolic acid (GA), and 4-
88 morpholinoethanesulfonic acid (MES) were purchased from Sigma-Aldrich (St. Louis, MO USA).
89 Ethylenediaminetetraacetic acid and disodium salt dihydrate (EDTA) were purchased from Fisher
90 Chemistry (MA, USA). N-hydroxysuccinimide (NHS) was purchased from Chem-Impex
91 International (IL, USA). (3-Aminopropyl) triethoxysilane, 98% (APTES), and 1-(3-
92 Dimethylaminopropyl)-3-ethylcarbodiimide (EDC) were purchased from Alfa Aesar (MA, USA).
93 Tryptone was purchased from IBI Scientific (IA, USA). Granulated yeast extract and Drisolv®
94 toluene anhydrous were purchased from EMD Millipore (USA). The viability/cytotoxicity assay
95 kit was purchased from Biotium (Fremont, CA USA). Solutions were made from Elga purelab flex
96 ultrapure deionized (DI) water (18.2 MΩ cm at 21°C). The POA1 bacteria was isolated from a
97 patient at the University of Washington.[31] All chemicals were used as received.

98 ***Electrode Preparation.*** Optically transparent electrodes (OTEs) were fabricated at Fraunhofer
99 USA Center for Coatings and Diamond Technologies (East Lansing, MI, USA). A boron-doped
100 diamond (BDD) microcrystalline film was deposited on a 2 mm thick quartz glass substrate by hot
101 filament chemical vapor deposition (CVD) and was cut into 1 cm^2 disks using a laser cutting
102 system. The BDD/OTE electrode was pretreated anodically in 1 M $NaClO_4$ (20 mA cm^{-2} for 20
103 min) to terminate it with -OH groups.[32] The pretreated BDD/OTE was rinsed sequentially with
104 ethanol, methanol, and water. Next, the cleaned BDD/OTE was placed in an Ar-filled glove box
105 and immersed in 5 mM APTES in anhydrous toluene for 3 hours. The APTES functionalized

106 BDD/OTE (APTES-BDD/OTE) was then rinsed three times with toluene and methanol and
107 annealed at 120°C for 30 min to promote cross-linking of the silanes.[33,34] The N-propyl-2-
108 hydroxyacetamide modified BDD electrode (OH-BDD/OTE) was prepared from an APTES-
109 BDD/OTE using GA and the EDC/NHS method. The chemical structure of the OH-BDD/OTE
110 functional group is shown in **Figure 1**. Details of the electrode functionalization methods are
111 provided in the Supporting Information (SI, **Figure S1**).

112 ***Electrode Characterization.*** The OTEs were characterized by CV, XPS (Kratos Axis-165),
113 and contact angle measurements. The CV scans were performed with two different ionic redox
114 couples (5 mM $K_3Fe(CN)_6/K_4Fe(CN)_6$ and 5 mM $Ru(NH_3)_6Cl_3/Ru(NH_3)_6Cl_2$ at 1:1 molar ratios) in
115 the PBS background electrolyte (pH = 7.4) to evaluate the charge transfer between the redox
116 couples and the OTE surfaces. The potential was swept at a scan rate of 100 mV s^{-1}. Contact angle
117 measurements were obtained by Image J software with DropSnake plugin.[35]

118 ***Bacteria Growth Media and Culture Conditions.*** The POA1 bacteria cells were transferred
119 from a stock solution and cultured in lysogeny broth (LB), which contained 10 g tryptone, 5 g
120 yeast extract, and 10 g NaCl in 1 L of DI water. The culture was incubated at 37° C on a rotary
121 shaker at 160 rotations per minute (rpm) for 16 hours, which corresponded to late-log phase of
122 bacteria growth.[36] After incubation, bacteria cells were washed three times in PBS by
123 centrifugation at 7000×g for 5 min at room temperature. The concentration of the bacteria in the
124 solution was quantified by optical density (OD) at 600 nm (OD_{600}). Direct plate counts were
125 performed, and a standard curve was constructed of OD versus plate count numbers (SI, **Figure**
126 **S2**). The bacteria cell concentration was determined to be approximately 1×10^9 cells mL^{-1} at an
127 OD_{600} value of 1.0.

128 ***Dual Staining Procedure.*** The bacteria counts were made with a viability/cytotoxicity assay
129 kit according to the manufacture's protocol (Biotium, USA). Prior to staining, bacteria were
130 washed three times with a 0.85% NaCl solution. The viability/cytotoxicity assay was prepared by
131 mixing 10 μL of DMAO, 20 μL of Ethidium Homodimer-III (EthD-III), and 80 μL of 0.85% NaCl.
132 DMAO is a green dye capable of staining nucleic acids in both intact and porated bacteria cells
133 (excitation 503 nm/ emission 530 nm). The EthD-III red dye (excitation 530 nm/ emission 620 nm)
134 selectively stains cells with a porated outer membrane. Mixed reagent solutions were prepared
135 freshly before each experiment. A 1 μL volume of reagent solution was added to each 100 μL of
136 PBS washed bacteria suspension. The bacteria were incubated in the reagent solution at room
137 temperature without light irradiation for 15 minutes. A cover slide was placed over the OTE after
138 staining and the cells were imaged at 10 individual random spots (128 by 128 μm area) using an
139 inverted fluorescent microscope (Olympus IX73, Japan) with band-pass filter sets, which have
140 blue wide pass with excitation 460-495 nm; emission 510-550 nm (FITC filter), and green wide
141 long pass with excitation 530-550 nm; emission 575 nm (TRITC filter).

142 ***Bacteria Attachment/Poration Studies.*** The POA1 cells were washed and resuspended in a
143 centrifuge tube with PBS to ~ 10^9 cells mL^{-1} and transferred to a 2 mL Teflon® cell for
144 attachment/poration studies (**Figure 2**). The OTEs were used as working electrodes and sealed at
145 the bottom of the SECM holder with an o-ring and a titanium foil was used as a current collector.
146 A Pt wire was used as a counter electrode and a Ag/AgCl electrode was used as a reference.
147 Potentials and currents were controlled and monitored with a bipotentiostat (CHI920D model, CH
148 Instrument, Inc). Each experiment was conducted for 105 minutes at a constant potential (-0.2 V
149 to 1.0 V vs. Ag/AgCl). For studying the effect of divalent cations on bacteria inactivation, different
150 concentrations of Mg^{2+} (5, 10, 15, 20 mM) were added into the PBS solution and cathodic/anodic

151 potentials were applied on the OTEs. Every experiment was repeated three times and all reported
152 errors and error bars represent the standard deviation about mean values.

153 ***Bacteria Surface Charge Measurements.*** The PAO1 zeta potentials were measured as a
154 function of solution conditions using electrophoretic light scattering (Nano-ZS, Malvern). The
155 POA1 cells (~ 10^9 cells mL^{-1}) were washed and resuspended in a 20 mL beaker with PBS. Small
156 amounts of EDTA or GA as chelators were added into the glass vial continuously by auto titration
157 (MPT-2, Malvern), and solution pH was monitored and recorded simultaneously. Solution phase
158 experiments were conducted with planktonic bacteria to determine the effect of GA and EDTA as
159 chelators in the presence of Mg^{2+} (0 - 30 mM).

160 ***Bacteria Titration Experiments.*** The titration experiments were conducted to determine the
161 charge regulation on the bacteria cell surface.[37,38] The bacteria were grown in the LB to stationary
162 phase. A concentration of ~1×10^{10} cells mL^{-1} was suspended in a beaker with 5 mL of 0.1 M NaCl,
163 which was adjusted to pH 11 by 0.1 N NaOH addition. The concentration of bacteria was
164 determined by OD_{600} as shown in Figure S2. A 0.1 N HCl solution was titrated into the beaker and
165 solution pH was monitored and recorded. Bacteria were transported continuously into disposable
166 capillary cells for surface potential measurements using a zetasizer (Nano-ZS, Malvern). The
167 titration results were used to estimate the dissociation constants (K_{a_i}) and their corresponding site
168 numbers (N_{a_i}) of acidic and basic functional groups on the bacteria cell surface. Details are shown
169 in the SI.

170 ***Quantum Mechanical Calculations.*** Density functional theory (DFT) calculations were
171 performed to determine the Gibbs free energy for adsorption of Mg^{2+} at the 2-hydroxyacetamide
172 functional group. Simulations were performed using Gaussian 16 software.[39] Unrestricted spin,
173 all-electron calculations were performed using the 6-31G+(d) basis set for geometry optimization,

frequency, and energy calculations. A scale factor of 0.9806 was used to correct for known systematic errors.[25] The gradient corrected Becke, three- parameter, Lee−Yang−Parr (B3LYP) functional was used for exchange and correlation. Implicit water solvation was incorporated using the SMD model.[40]

Mathematical Model. To interpret bacteria poration, chelation of metallic ions on the cell surface, and surface charge measurements, we developed a mathematical model based on the nonlinear Poisson-Boltzmann Equation, which estimates the distribution of counter ions near the charged cell surface.[41] Using the Henderson-Hasselbalch equation for PBS, GA, and EDTA under different pH conditions, the model accounts for protonation/deprotonation of acidic groups, and chelation of divalent cations at fixed sites on the cell surface. We assumed that these cations are subject to both an attractive non-electrostatic and electrostatic interaction potential from the cell membrane.[42] We also hypothesized that bacterial surface charges arise from carboxylic, hydroxyl, and phosphoric groups, which yield the pH dependence.[38]

Ignoring the radius of curvature of the cell surface and considering the cell surface as a flat ion-penetrable layer with finite thickness (r_d), where there are not any basic groups, we described the electric potential distribution with respect to distance from the cell surface by:[42]

$$\frac{d^2y}{dx^2} = \begin{cases} -\rho - c_0 \sum_i z_i n_i e^{(-z_i y)}, & x < x_d \\ -c_0 \sum_i z_i n_i e^{(-z_i y)}, & x \geq x_d \end{cases} \quad (1)$$

where $y = e\,\psi/kT$ and ψ are the dimensionless and dimensional electric potentials, respectively; e is the charge of an electron; kT is the thermal energy; $x = r/\kappa$ is the dimensionless distance from the ion-impenetrable core of the cell surface; $x_d = r_d/\kappa$; $\kappa = \sqrt{(\epsilon_w \varepsilon_0 kT)/(e^2 N_A \sum_i z_i^2 n_i)}$ is the Debye-Huckel length; n_i is the molar concentration of ions of type i; N_A is the Avogadro's

number; z_i is the valence of ions of type i; ϵ_w is the dielectric constant of the bulk; ε_0 is the permittivity of the vacuum; and $c_0 = (\kappa^2 e^2 N_A)/(\epsilon_w \varepsilon_0 kT)$.

In equation (1), ρ is the density of static charges in the ion-penetrable layer of the cell surface, which can be defined by protonation and deprotonation of ionizable acidic groups according to the following equilibrium reactions:[38,42,43]

$$\mathrm{R}_{a_i}\mathrm{H} \leftrightharpoons \mathrm{R}_{a_i}^{-} + \mathrm{H}^{+} \tag{2}$$

and the adsorption of divalent cations is given by:[38]

$$\mathrm{R}_{a_i}\mathrm{M}^{+} \leftrightharpoons \mathrm{R}_{a_i}^{-} + \mathrm{M}^{2+} \tag{3}$$

where $\mathrm{R}_{a_i}^{-}$ indicates ionizable acidic groups of type i, namely, phosphoric, carboxylic, and hydroxyl groups, and M^{2+} represents the divalent cations. The static charge density in the ion-penetrable layer is given by:

$$\rho = \frac{\kappa^2 e^2}{kT\epsilon_0\epsilon_w}\left\{-\sum_i \frac{N_{a_i}K_{a_i}}{k_{a_i} + [\mathrm{H}^+]e^{-y} + \frac{K_{a_i}}{K_M}[\mathrm{M}^{2+}]e^{-2y}} + \frac{\frac{K_{a_i}}{K_M}[\mathrm{M}^{2+}]e^{-2y}}{k_{a_i} + [\mathrm{H}^+]e^{-y} + \frac{K_{a_i}}{K_M}[\mathrm{M}^{2+}]e^{-2y}} - 2\frac{[\mathrm{H_2Y}^{2-}]N_d e^{2y-\Delta g}}{1 + [\mathrm{H_2Y}^{2-}]e^{2y-\Delta g}}\right\} \tag{4}$$

where the last term represents adsorption of $\mathrm{H_2Y}^{2-}$ on to the ion-penetrable layer, and chelation of a metallic ion by the displacement of the weakly acidic protons using a modified Langmuir isotherm,[42,44,45] as shown in **Figure 3**. The adsorption is occurring according to the following reaction:

$$\mathrm{M}^{2+} + \mathrm{H_2Y}^{2-} \leftrightharpoons \mathrm{MY}^{2-} + 2\mathrm{H}^{+}. \tag{5}$$

In equation (4), $[H^+]$, $[M^{2+}]$, and $[H_2Y^{2-}]$ are the concentrations of the hydrogen ions, divalent cations, and dissociated divalent chelator anions, respectively; N_{a_i} and N_d are the number of acidic sites of type i, and adsorption sites for chelation per unit volume, respectively; K_{a_i} and K_M are dissociation constants of acidic group of type i and binding constants of adsorbed divalent cations, respectively; and Δg is the Gibbs energy of specific interaction nondimensionalized by kT.

Equation (1) is subjected to the following boundary conditions

$$\left.\frac{dy}{dx}\right|_{x=0} = 0, \quad y|_{x=\infty} = \left.\frac{dy}{dx}\right|_{x=\infty} = 0, \quad \lim_{x\to x_d^+} y = \lim_{x\to x_d^-} y, \tag{6}$$

where $x = 0$ indicates the ion-impenetrable core of the cell surface, and $x = \infty$ represents the bulk solution. Using the finite difference scheme with the direct discretization of the derivative terms, we solved equation (1) numerically to find dimensionless zeta potential, y, where we applied the boundary conditions in equation (6) via a shooting method, and assumed the thickness of ion-penetrable layer to be $r_d = 5$ nm. We used a fully nonlinear optimization to find the model parameters (N_{a_1} to N_{a_4}, N_d, K_{a_1} to K_{a_4}, K_M, and Δg) by fitting the zeta potentials from the model to those from the experimental measurements.

Results and Discussion

Electrode Characterization. Two different electrode surfaces (i.e., BDD/OTE and OH-BDD/OTE) were characterized using CV scans to determine the effect of surface functional groups on the charge transfer reactions with aqueous ionic redox couples (**Figure 4**). The CV scans were used to assess the charging currents on the BDD/OTE and OH-BDD/OTE in the PBS electrolyte, which is a well-established method to estimate the reactive surface area.[46,47] The average charging currents on BDD/OTE and OH-BDD/OTE were 29 μA and 16 μA, respectively, at a potential of 0 V vs. Ag/AgCl (**Figure 4a**). These results indicated that the reactive surface area decreased by ~ 45% after electrode modification, likely due to a blockage of active sites by the functionalization

process. Therefore, more work is needed to develop these coatings so that reactive surface area is not compromised, but the bacteriostat properties of the coatings are anticipated to prevent biofilm growth, which if not addressed can result in the complete blockage of the electrode surface. CV scans containing 5.0 mM of the $Fe(CN)_6^{3-/4-}$ inner sphere redox couple showed a lower current for the OH-BDD/OTE relative to the BDD/OTE and a positive shift in the formal electrode potential (**Figure 4b**). These results were attributed to repulsive electrostatic interactions between the anionic redox couple and the negative dipoles of the oxygen atoms in the 2-hydroxyacetamide functional groups. Thereby, increasing the surface concentration of the oxidized redox species relative to the reduced one. The charge transfer of the $Fe(CN)_6^{3-/4-}$ inner sphere redox couple is very sensitive to surface termination of the electrodes.[48–50] By contrast, the peak current was only slightly reduced at the OH-BDD/OTE relative to the BDD/OTE with the 5 mM $Ru(NH_3)_6^{2+/3+}$ redox couple (**Figure 4c**). The results indicated that the $Ru(NH_3)_6^{2+/3+}$ outer sphere redox couple was less sensitive to electrostatic interactions than the inner sphere redox couple.[51] Also, the peak separation of both redox couples were approximately the same for both electrodes, indicating that only access of the redox couples to the electrode surface were affected and that the charge transfer kinetics were not greatly affected by the functionalization process. The BDD/OTE had a hydrophilic surface,[52] with a measured contact angle of 45 degrees (**Figure 4d**). The OH-BDD/OTE electrode had a more hydrophobic surface with a measured contact angle of 65 degrees (**Figure 4d**).

To determine the stability of the electrode modification under the potential range of the experiments (-0.2 to 1.0 V vs. Ag/AgCl), CV scans were performed for the OH-BDD/OTE after a total anodic charge of 256 C and cathodic charge of -129 C were applied to the electrode. The CV scans showed similar results for the $Fe(CN)_6^{3-/4-}$ and $Ru(NH_3)_6^{2+/3+}$ redox couples before and after

260 this "ageing" process (SI, Figure S-3), indicating that the surface modification was stable in the
261 potential range of -0.2 to 1.0 V vs. Ag/AgCl.

262 The surface chemistry of the OTEs were analyzed by XPS and results are shown in **Figure 5**
263 and **Table 1.** The C1s spectrum assignments were based on previous literature data.[53] The
264 BDD/OTE contained primarily C-H (C1 = 42%), C-C (C2 = 21%), and C-OH (C4= 19%)
265 functionalities. By contrast, a significant proportion of the C-C (C2 = 93.2%), C-O/C=O/-
266 $(CH_2CH_2NH)_n$- (C3 = 4.2%), and -COOH (C5 = 2.6%) groups were detected on the OH-BDD/OTE.
267 The peak area ratios for C/O, C/N, and C/Si are shown in **Table 1b**. The C/O ratios were similar
268 for both OTEs (5.9 for BDD/OTE and 4.1 for OH-BDD/OTE), but the C/N ratios (59.5 for
269 BDD/OTE and 17.2 for OH-BDD/OTE) and C/Si ratios (64.5 for BDD/OTE and 17.4 for OH-
270 BDD/OTE) decreased due to 2-hydroxyacetamide functionalization. Comparing the C/N and C/Si
271 ratios before and after functionalization provided an estimate of ~ 77% surface coverage of the 2-
272 hydroxyacetamide functional groups on the BDD surface (see SI for details).

273 ***Bacteria Attachment/Poration Studies.*** Results for bacteria attachment numbers and the
274 percentages of porated cells as a function of the applied potential on the OTEs are shown in **Figure**
275 **6a** and **Figure 6b**, respectively. These values were determined by averaging the direct count of 10
276 random locations on each sample. Initially, approximately 10^9 cells mL^{-1} were suspended in the
277 bulk solution with a total solution volume of 2 mL. The currents on both OTEs were similar, but
278 the attached cell numbers were higher on the OH-BDD/OTE, except for applied potentials of 0.8
279 and 1.0 V vs Ag/AgCl **(Figure 6a)**. These results suggested that the functionalization of the OH-
280 BDD/OTE provided additional adsorption sites for bacteria, possibly due to a higher
281 hydrophobicity. However, at the higher anodic potentials, the formation of oxygen bubbles likely
282 offsets this difference.

283 The attached cells were analyzed for their membrane integrity using fluorescent microscopy
284 (**Figure 6b)**. In general, the percentage of bacteria with membrane damage increased upon
285 increases in anodic and cathodic potentials on the BDD/OTE (**Figure 6b**). These results were
286 attributed to basic and acidic local pH environments due to water electrolysis under cathodic and
287 anodic potentials, respectively, and the formation of ROS and reactive chlorine species.[18] However,
288 two- to three-fold higher percentage of porated bacteria were observed on the OH-BDD/OTE
289 compared with BDD/OTE under applied anodic potentials between 0.1 to 0.5 V vs Ag/AgCl
290 **(Figure 6b)**, suggesting that other mechanisms may be responsible for bacteria inactivation under
291 these conditions.

292 One possible mechanism for destabilization of the bacteria membrane is chelation of the
293 divalent cations from charge balancing sites. The cell membrane consists of $-COO^-$, $-HPO_4^-$, and -
294 PO_4^{2-} functional groups on the polyanionic LPS,[54] which are neutralized and mechanically
295 stabilized by divalent cations such as Ca^{2+} and Mg^{2+}.[55] The structure of the 2-hydroxyacetamide
296 functional group on the OH-BDD/OTE provides a possible site that can chelate divalent cations
297 from the LPS and cause bacterial membrane damage. DFT simulations were performed to provide
298 evidence for the existence of this chelation site. The Gibbs free energy for adsorption of Mg^{2+} at
299 the 2-hydroxyacetamide functional group was calculated as ΔG = -180 kJ mol^{-1} (**Figure 7**). These
300 results support the hypothesis that divalent cation chelation by the OH-BDD/OTE was
301 thermodynamically favorable.

302 However, the DFT results do not provide evidence that this chelation effect is strong enough
303 to remove divalent cations from the LPS. To support this possibility, various Mg^{2+} concentrations
304 were added into the 2 mL Teflon® cell under applied potentials of 0.2 V and -0.15 V vs. Ag/AgCl
305 for both the BDD/OTE and OH-BDD/OTE (**Figure 8**). The results in **Figure 8a** show that under

306 an applied anodic potential of 0.2 V vs. Ag/AgCl and in the absence of Mg^{2+}, the percentage of
307 viable bacteria, which is defined as bacteria with uncompromised cell membranes, was 82 ± 2.0%
308 on the BDD/OTE and 53.3 ± 1.7% on the OH-BDD/OTE. Upon the addition of Mg^{2+} to solution
309 (5 to 15 mM) the percentage of viable bacteria significantly increased for both OTEs (**Figure 8a**).
310 The percentage of viable bacteria increased from 53.3 ± 1.7% to 92.4 ± 2.7% on the OH-BDD/OTE
311 and increased from 82 ± 2.0% to 89 ± 3.3% on the BDD/OTE. This result may be due to the ability
312 of the additional Mg^{2+} ions to stabilize the cell membrane. By contrast, upon the addition of Mg^{2+}
313 to solution with a polarization of -0.15 V vs. Ag/AgCl, the percentage of viable bacteria
314 significantly increased from 55 ± 4.1% % to 75 ± 4.5% on BDD/OTE, but was approximately
315 constant on the OH-BDD/OTE with and without the presence of Mg^{2+} (**Figure 8b**). For example,
316 the percentage of viable bacteria was 55 ± 5.02% on the OH-BDD/OTE without the addition of
317 Mg^{2+} and were 62.4 ± 4.8%, 60.0 ± 4.5%, and 57.9 ± 4.2% with Mg^{2+} concentrations of 5, 10, and
318 15 mM, respectively (**Figure 8b**). These results suggest that both the applied potential and the
319 Mg^{2+} concentration both play roles in the bacteria poration process. It is hypothesized that when
320 the OTE is polarized as a cathode, the electric double layers of the adsorbed POA1 cells and the
321 OTEs begin to overlap .[56] Therefore, there is a three-way competition for Mg^{2+} ions between the
322 2-hydroxyacetamide chelation sites, PAO1 bacteria, and the OTE double layer. Apparently under
323 cathodic conditions the Mg^{2+} ions are more thermodynamically favorable (or kinetically trapped)
324 at the chelation sites and OTE double layer over the PAO1 surface. It was beyond the scope of
325 work to investigate this mechanism in further detail in this study. However, more experimental
326 and theoretical work is needed to test the proposed hypothesis.

327 To support the chelation hypothesis by the 2-hydroxyacetamide functional group of the OH-
328 BDD/OTE, solution-phase experiments were conducted by adding different concentrations of

329 either GA or EDTA to solutions containing bacteria. GA was used as a solution phase surrogate
330 for the 2-hydroxyacetamide functional groups and EDTA was used for comparison purposes, as it
331 is a well-known chelator.[23,57]

332 Bacteria numbers were controlled by OD_{600} readings before each experiment. As shown in
333 **Figure 9**, in general, the percentage of viable bacteria decreased with increases in the concentration
334 of chelator from 0 to 20 mM. The percentage of viable bacteria decreased from 77 ± 1.5% to 45 ±
335 2.0% when the concentration of GA was increased from 0 to 20 mM (**Figure 9a**), and the
336 percentage of viable bacteria decreased from 75 ± 1.5% to 35 ± 2.3% over the same concentration
337 range for EDTA (**Figure 9b**). The results indicated that GA behaved similarly to the well-known
338 EDTA chelator and supports the hypothesis that the 2-hydroxyacetamide functional groups can act
339 as a chelator of divalent cations.

340 For a deeper understanding of the effects that the solution phase chelators and divalent cations
341 have on the bacteria surface charge, zeta potential measurements were made during the addition
342 of EDTA or GA into solution in the presence of different Mg^{2+} concentrations (i.e., 0-30 mM).
343 The POA1 bacteria surface charge was around -13 mV in the PBS electrolyte (pH = 7.5) in the
344 absence of either chelators or added divalent cations (**Figure 10a**). However, the bacteria surface
345 charge became more negative upon the addition of EDTA in the absence of Mg^{2+} and reached a
346 value of -18 mV at a concentration of 30 mM EDTA (**Figure 10a**). The addition of Mg^{2+} (10, 20
347 and 30 mM) resulted in similar zeta potential versus EDTA concentration profiles, but they were
348 shifted to higher surface charge values at a given EDTA concentration (**Figure 10b-d)**. The
349 solution pH dropped from 7.5 to 5.5 while 30 mM EDTA was titrated into the system (data not
350 shown). The zeta potential dropped to -22 mV once cell lysis occurred and a white precipitate was
351 observed (data not shown).

352 The same experiments were conducted using GA as a chelator and similar experimental trends
353 were observed (**Figure 11**). The POA1 bacteria zeta potential was around -12 mV in the PBS
354 electrolyte (**Figure 11a**). The zeta potential decreased to -16 mV upon the progressive addition of
355 GA in the absence of Mg^{2+}. Additional Mg^{2+} (10, 20 and 30 mM) increased the cell surface zeta
356 potential as shown in **Figures 11b-d**. Similar to the EDTA experiments, the cell surface potentials
357 decreased when GA was titrated into solution. Consequently, the solution pH dropped from 7.5 to
358 3.5 while 30 mM GA was titrated into the system (data not shown). These results indicated that
359 the bacteria surface charge increased with an increase in the concentration of divalent cations and
360 that high enough concentrations of either EDTA or GA could chelate these ions, leading to
361 decreases in surface charge and eventually cell lysis.

362 A mathematical model was used to interpret the experimental zeta potential measurements as
363 a function of solution conditions. The dissociation constant (K_{a_i}), and the corresponding site
364 number (N_{a_i}) of acidic functional groups for bacteria were determined from experimental titration
365 data (SI, **Figure S4**). Previous titration studies demonstrated that bacteria have four primary
366 acid/base functional groups including carboxylic, phosphate, amine, and hydroxyl groups.[38,58] In
367 our titration study (as shown in **Figure S4**) the results demonstrated that POA1 has four pK_{a_i}
368 values of 3.9, 7.4, 8.6 and 10.6 with their corresponding site numbers of 6.5, 5.4, 8.3 and 16.1
369 number/nm^2, as shown in the first row of **Table 2**. The mathematical model was also used to
370 optimize N_{a_i} and pK_{a_i} values by fitting simulated zeta potentials to those from experimental
371 measurements. Table 2 compares optimized POA1 N_{a_i} and pK_{a_i} values obtained from the model
372 with those from the experimental measurements, where three of the four pK_{a_i} values were closely
373 matched. The model also predicts Gibbs free energy of chelation and the corresponding N_{a_i} for
374 EDTA and GA under various divalent cation concentrations. Overall, parameters predicted by the

375 model are in the same order of magnitude and reasonable agreement with the experimental
376 measurements (sum of squared residuals for dimensionless zeta potential, y, were 9.3x 10^{-3}, 2.7 x
377 10^{-2}, 2.3 x 10^{-2}, and 2.1 x 10^{-2}, for EDTA with 0, 10, 20, and 30 mM Mg^{2+}, respectively, and 1.1 x
378 10^{-2}, 1.7 x 10^{-2}, 1.5 x 10^{-2}, and 1.2 x 10^{-2} for GA with 0, 10, 20, and 30 mM Mg^{2+}, respectively).
379 **Figure 10** and **11** compare zeta potentials obtained from experimental measurements and
380 simulations for EDTA and GA, respectively. The reasonable agreement between experimental data
381 and the mathematical model supports the chelation mechanism as a viable explanation for PAO1
382 poration in our studies.

383 **Conclusions**

384 The BDD electrode surface was successfully modified with 2-hydroxyacetamide functional
385 groups. CV scans of $Fe(CN)_6^{3-/4-}$ and $Ru(NH_3)_6^{2+/3+}$ redox couples confirmed that the reactive
386 surface area decreased by ~ 45% after electrode modification, likely due to a blockage of active
387 sites by the functionalization process. XPS measurements confirmed the functional groups on the
388 OTEs. The bacteria poration ratio on the OH-BDD/OTE surface was generally higher than on the
389 BDD/OTE surface, which was attributed to chelation of divalent cations from the POA1 cell
390 membrane leading to poration. Solution phase experiments with POA1, Mg^{2+}, and GA as a model
391 chelator supported this chelation mechanism, which was corroborated with DFT simulations and
392 a mathematical model based on the nonlinear Poisson-Boltzmann equation. Further work is needed
393 to minimize the decrease of reactive surface area upon electrode modification and determine the
394 interaction of bacteria cells on polarized electrode surfaces under complex solution conditions and
395 in the presence of various surface functional groups. BDD was used as a model electrode, due to
396 its inert surface, chemical stability, and ability to fabricate as an OTE to facilitate the experimental
397 work. However, in practice the BDD electrode may be replaced with other electrode materials,

since the modification occurs through a self-assembly process via reaction with -OH groups on the electrode surface. Therefore, the modification is appropriate for carbon and metal oxide electrodes, and thus should have applicability on a range of electrode materials.

Supporting Information

Experimental methods description; Bacteria quantitation versus OD_{600}; CV scans; Bacteria titration results

Corresponding Author

*E-mail: chaplin@uic.edu

Acknowledgements

Funding for this work was provided by two National Science Foundation awards to B.P. Chaplin (CBET-1453081; CBET-1604776).

409 **Figures and Tables.**

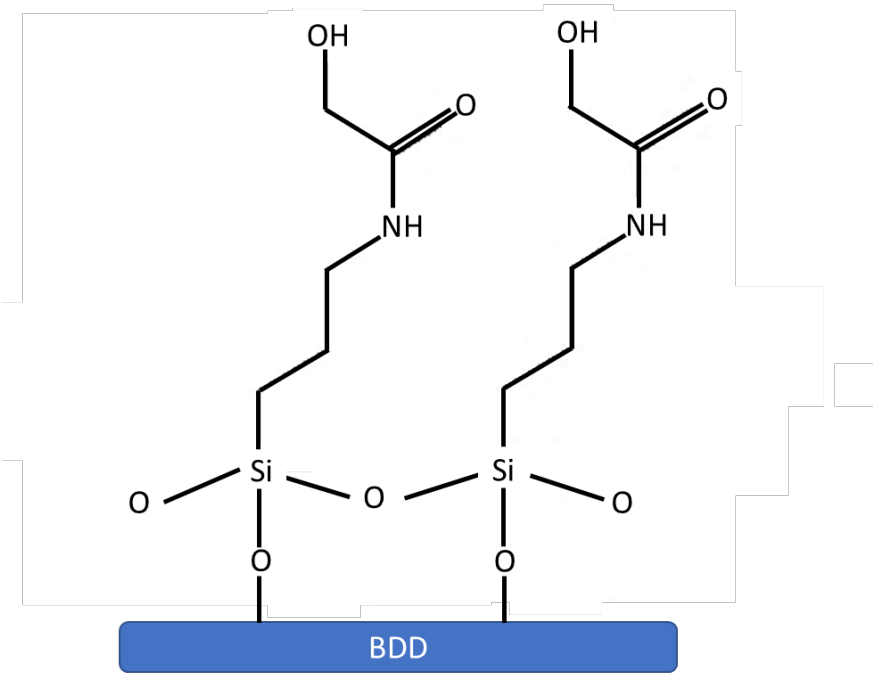

410

411 **Figure 1.** The structure of N-propyl-2-hydroxyacetamide modified BDD (OH-BDD/OTE).

412

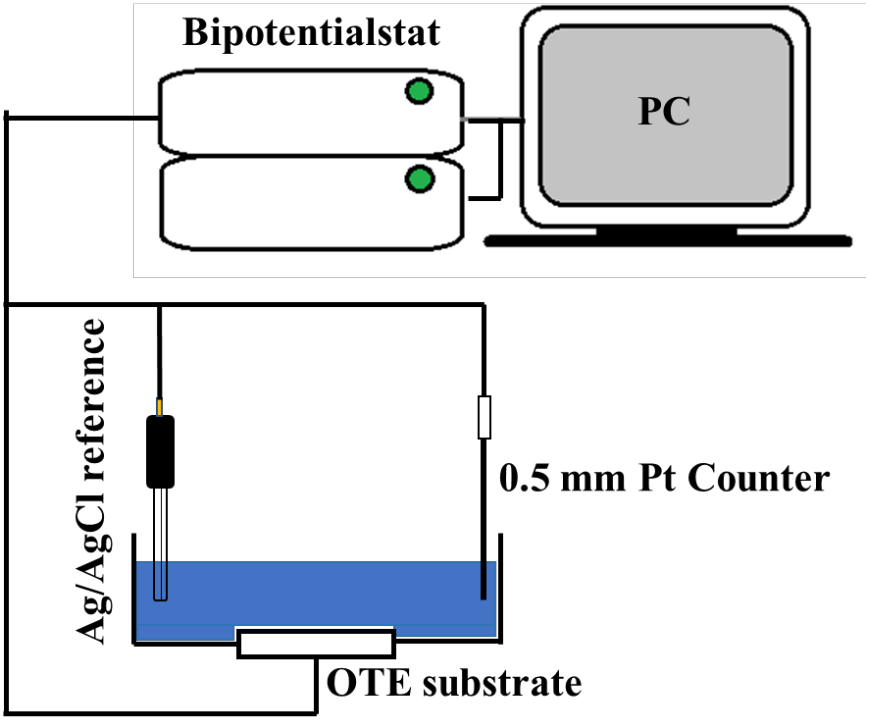

Figure 2. Experiment setup including OTE substrate, reference electrode and platinum counter electrode with bipotentiostat.

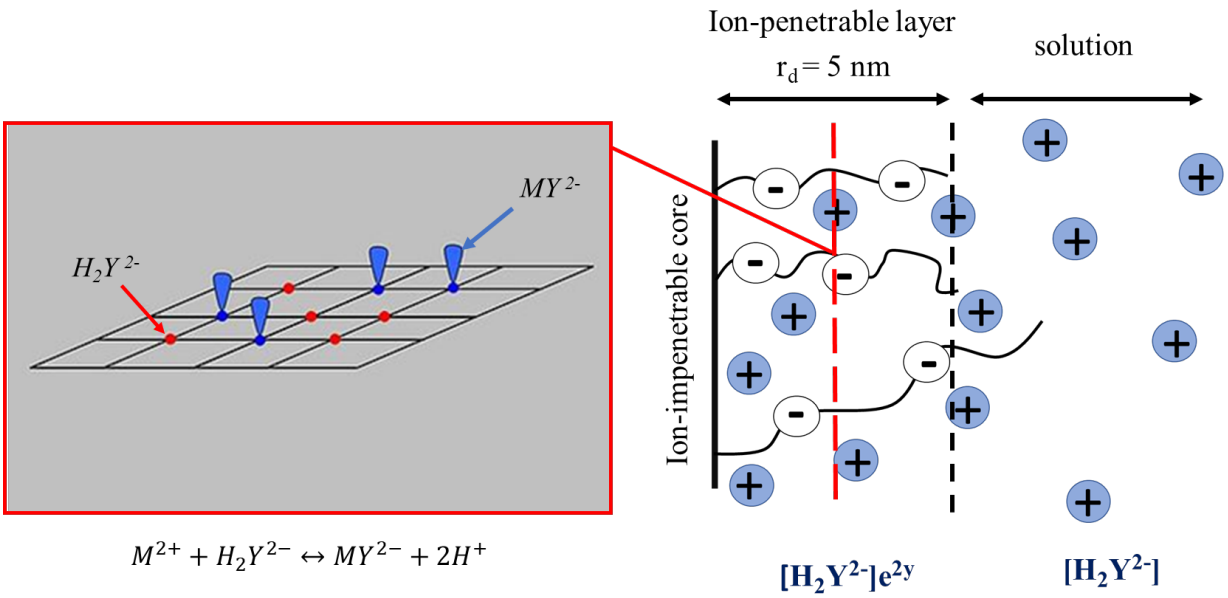

Figure 3. Schematic presentation of a charge profile of bacteria surface and divalent ions binding sites in the ion-penetrable layer. Left panel: red circles represent binding sites occupied by protons and blue symbols represent binding sites where a M^{2+} cation is present.

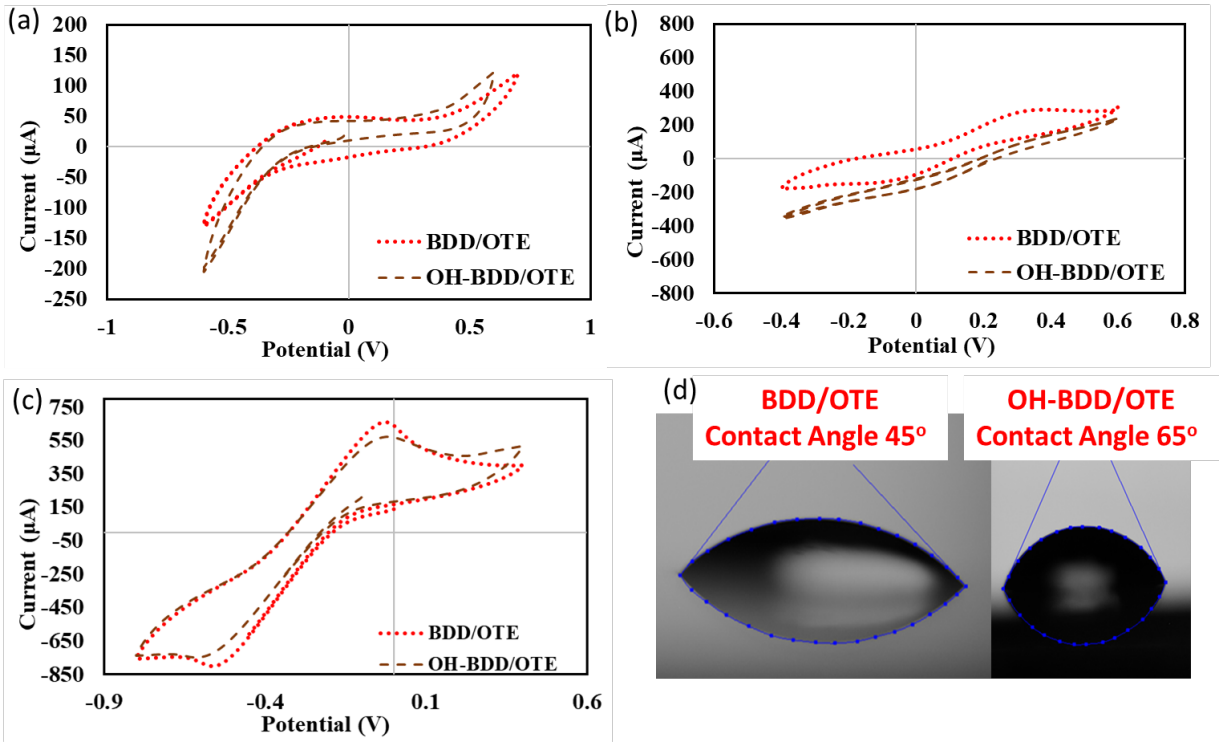

Figure 4. Cyclic voltammogram (CV) curves of bare BDD/OTE and OH-BDD/OTE in the (a) phosphate buffer saline (1x PBS), pH = 7.4 (b) PBS containing 5 mM $K_3Fe(CN)_6/K_4Fe(CN)_6$ and (c) PBS containing 5mM $Ru(NH_3)_6Cl_3/Ru(NH_3)_6Cl_2$. (V vs Ag/AgCl) (d) contact angles of BDD/OTE and OH-BDD/OTE. PBS composition: NaCl = 138 mM, KCl = 2.7 mM, Na_2HPO_4 = 10 mM, KH_2PO_4 = 1.8 mM.

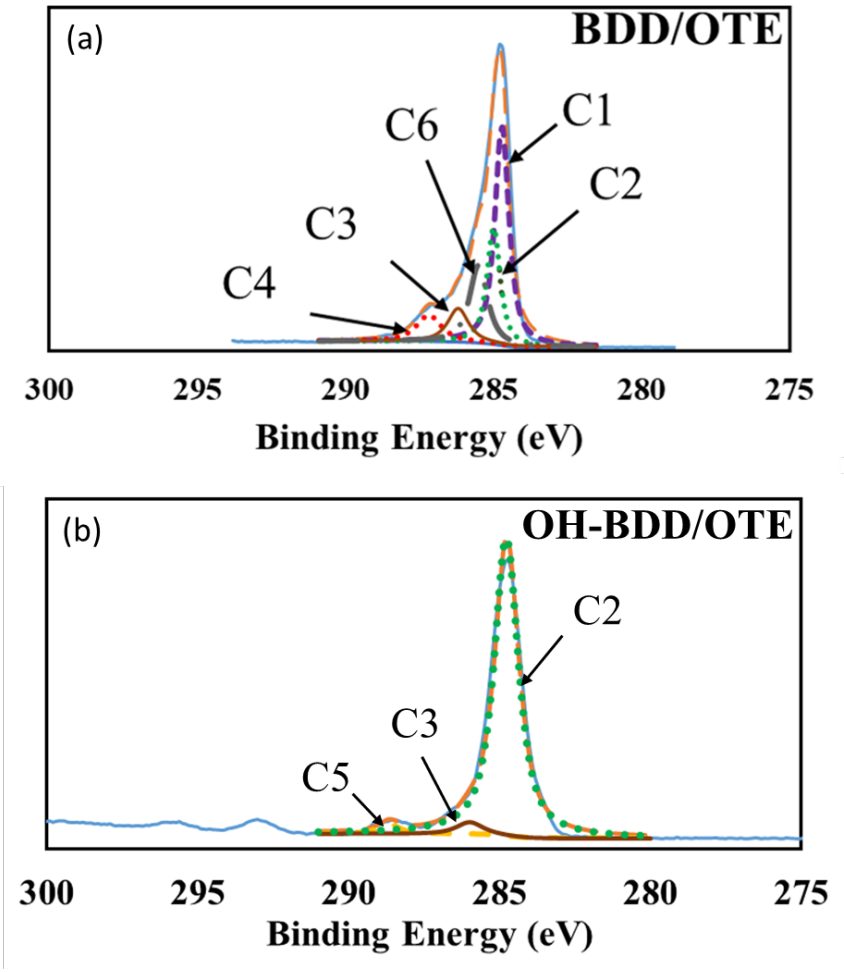

Figure 5. XPS spectra analysis of (a) BDD/OTE and (b) OH-BDD/OTE. C1 purple, C2 green, C3 brown, C4 red, C5 yellow, C6 grey and orange line for total peak area.

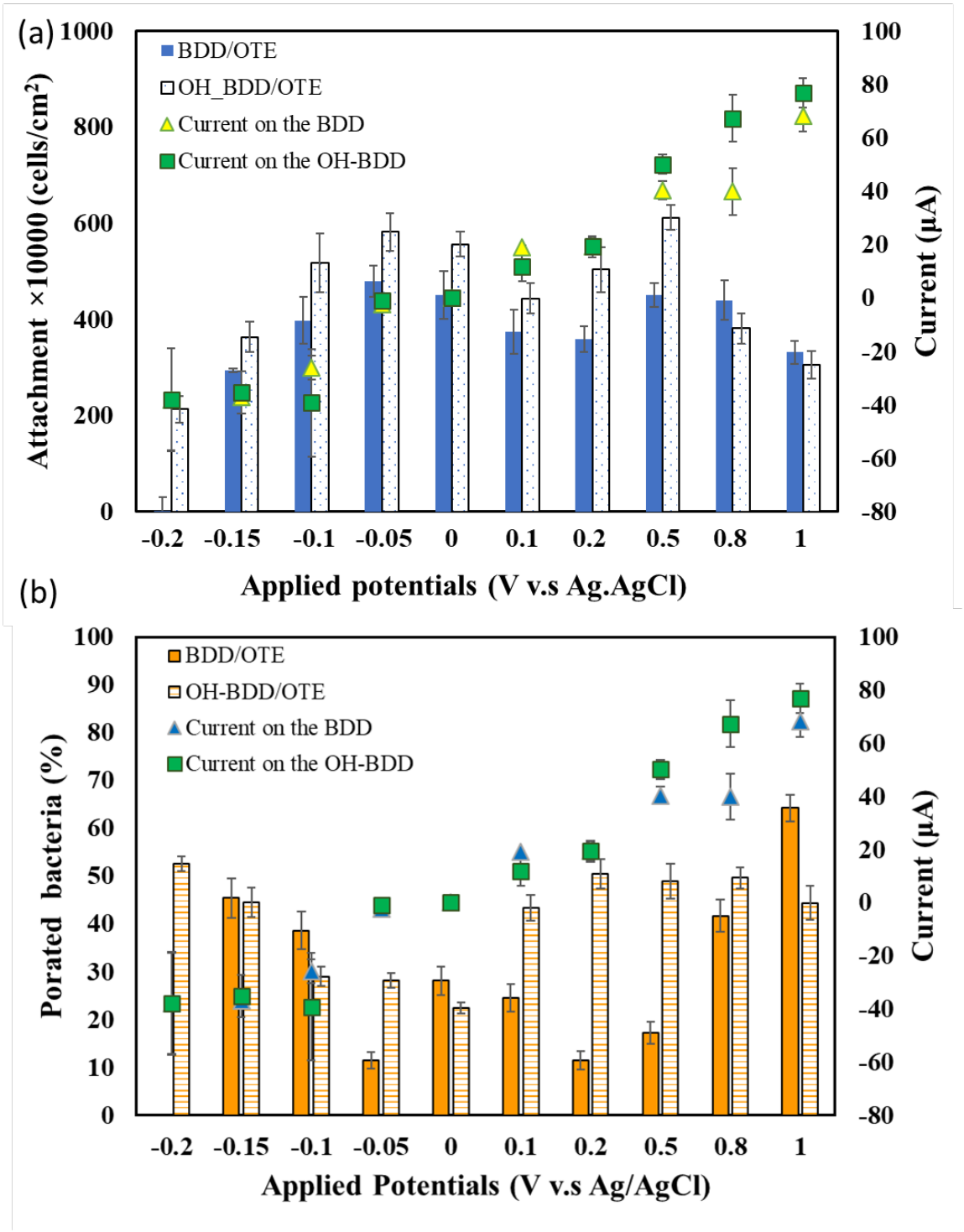

Figure 6. Comparison of the (a) bacteria total attachment number and (b) percentage of porated bacteria (bars) on the two different substrates as a function of the applied potential. Measured currents given as data points.

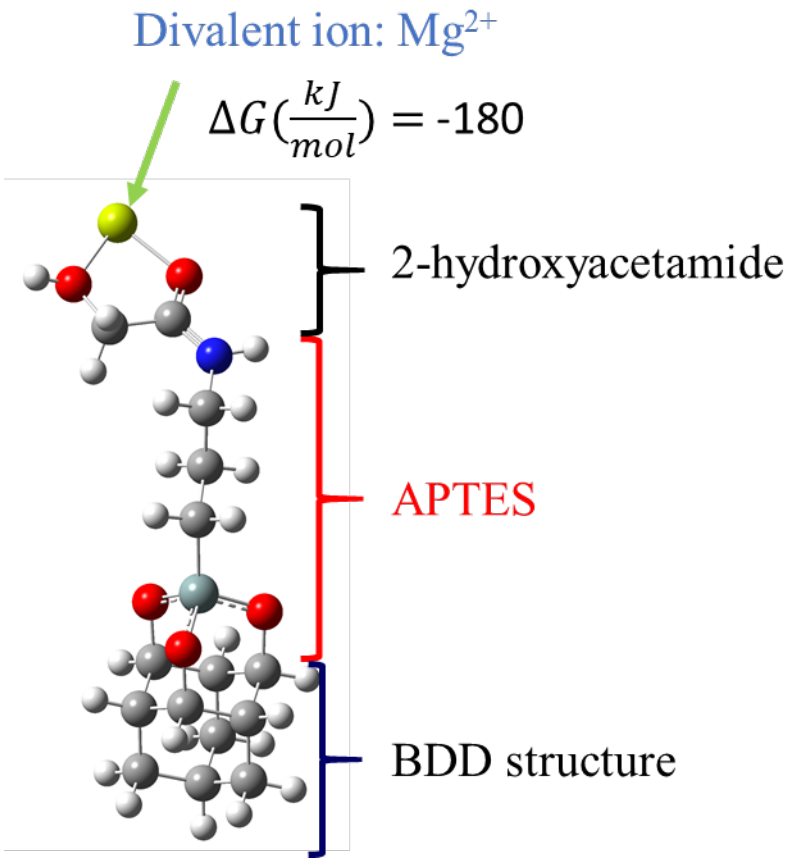

Figure 7. Optimized geometry of adsorption of Mg^{2+} at the 2-hydroxyacetamide functional group of the OH-BDD/OTE determined by DFT simulations. Atom key: Oxygen = red; Carbon = gray; Nitrogen = blue; Silicon = dark-grey; Magnesium = yellow; Hydrogen = white.

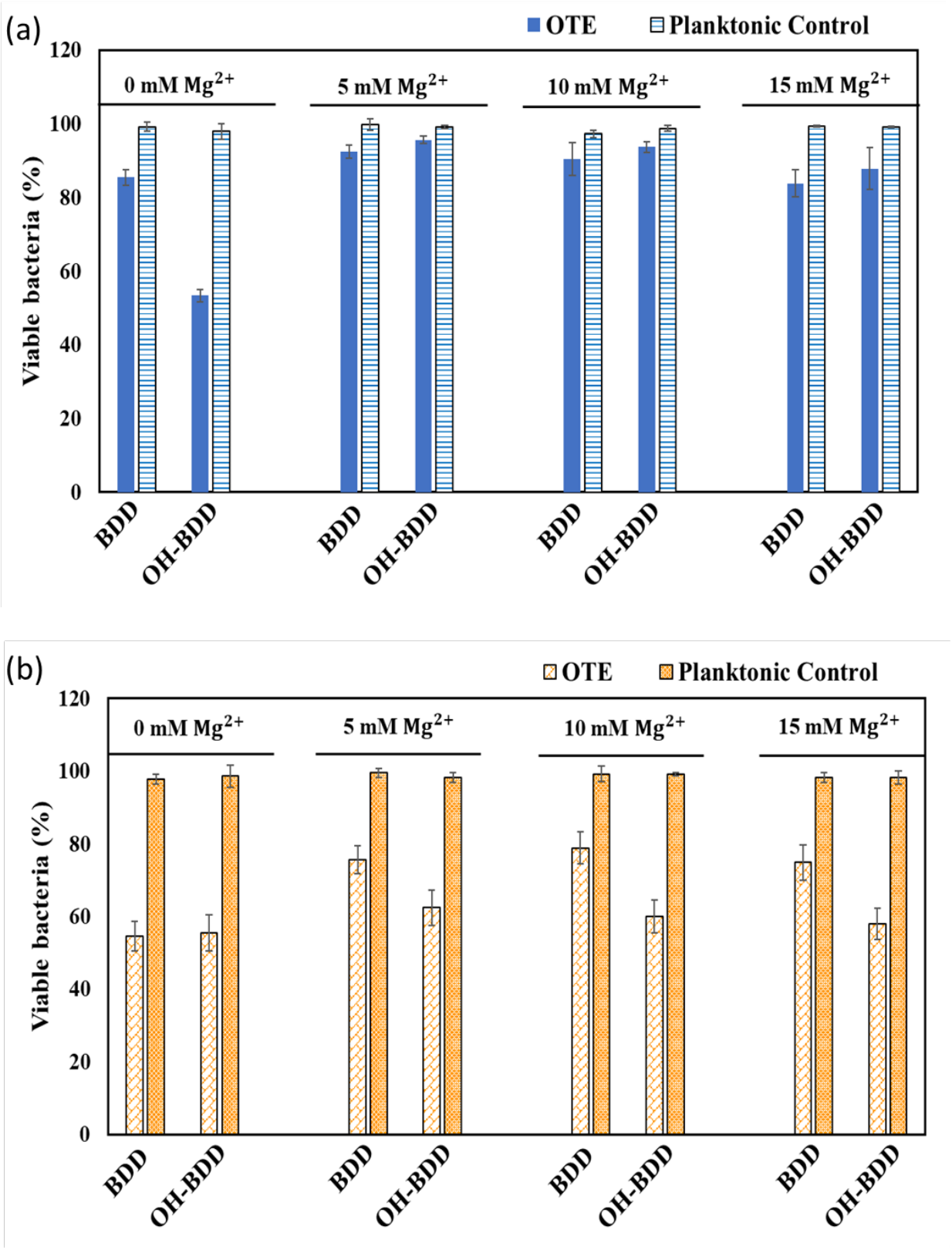

Figure 8. Comparison of POA1 viable ratio on the different substrates with different concentration of $MgCl_2$ when the applied potential was (a) 0.2V and (b) -0.15V (n = 3).

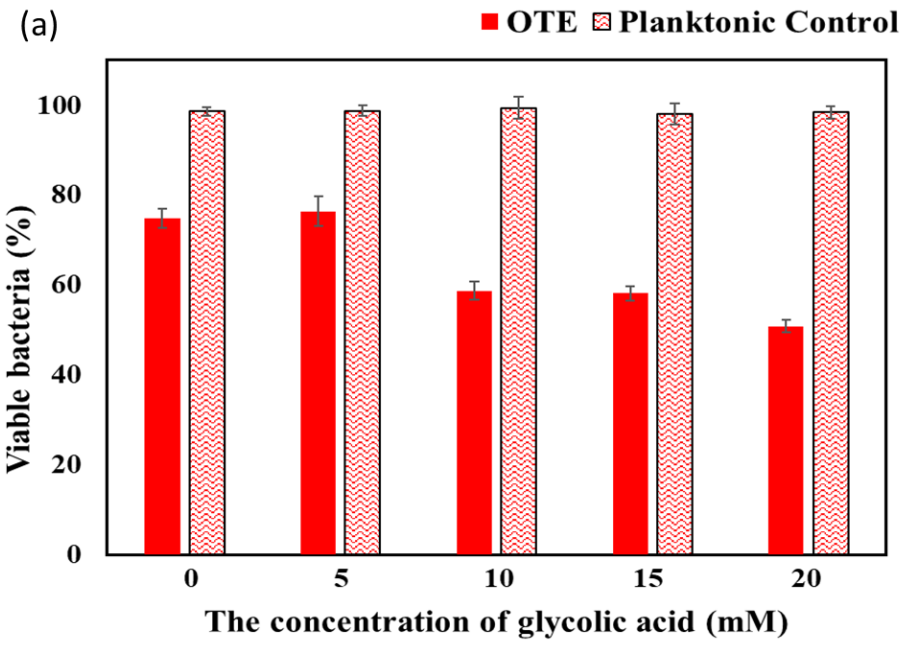

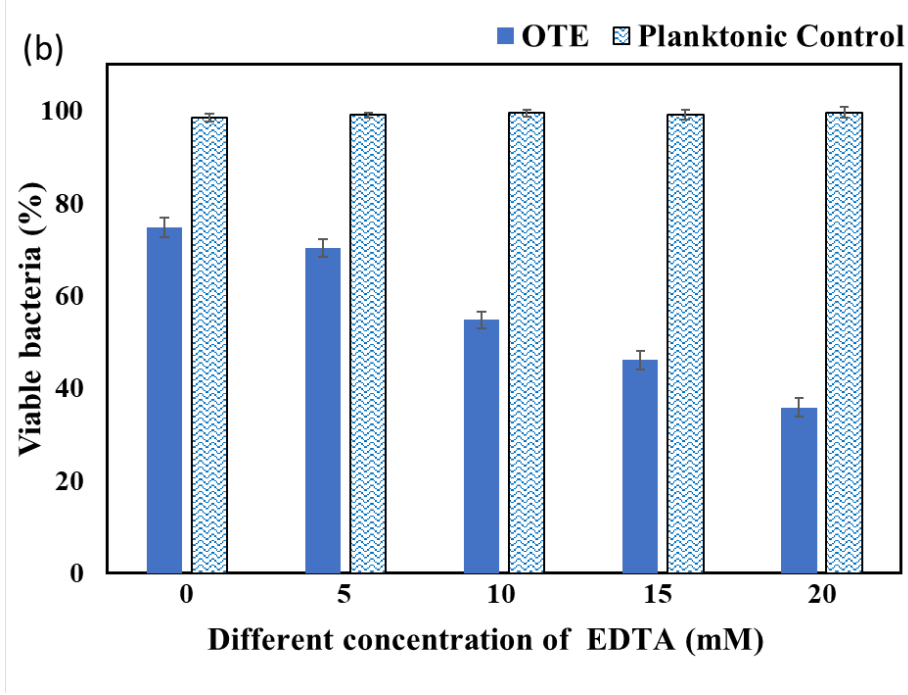

Figure 9. Comparison of the percentage of viable bacteria under different concentrations of (a) glycolic acid (GA) and (b) EDTA without applied potential (n = 3). All experiments used planktonic bacteria. Bacteria cells were exposed to different concentrations of EDTA and GA solutions for 90 minutes.

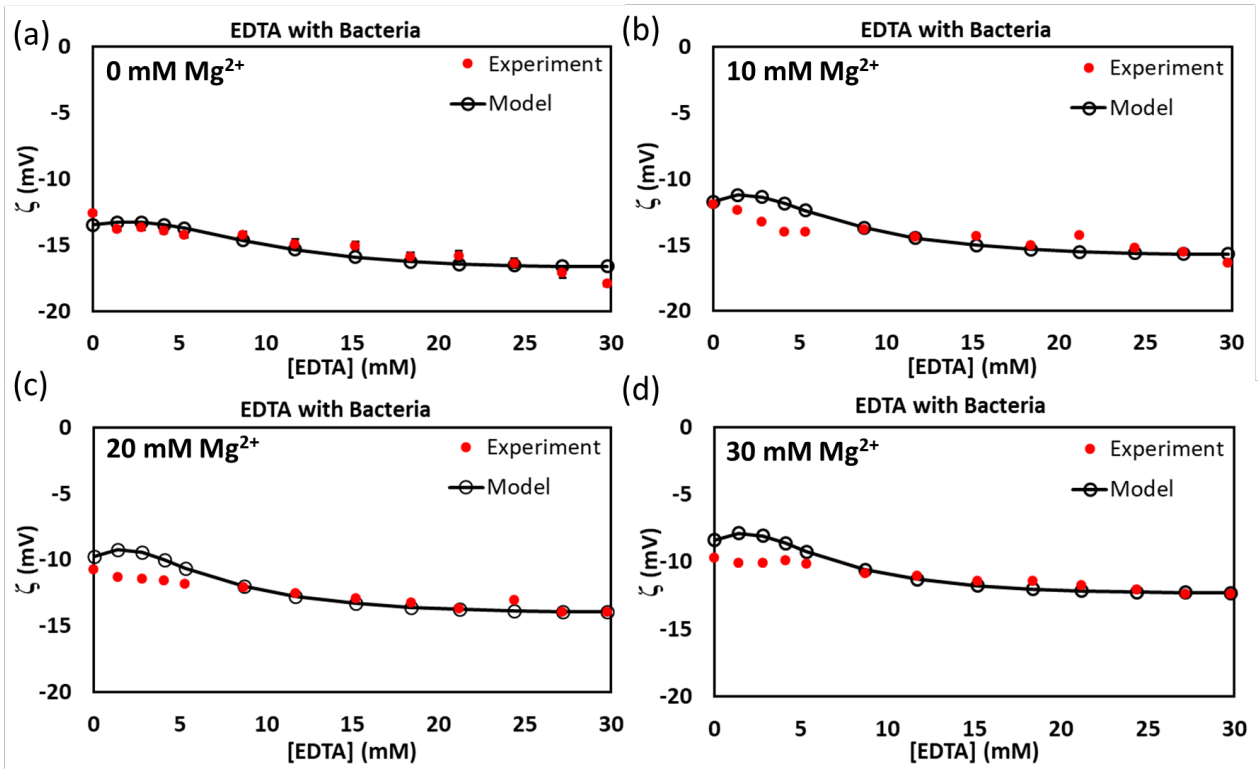

Figure 10. Zeta potential of POA1 as function of different EDTA concentrations and (a) 0 mM, (b) 10 mM, (c) 20 mM and (d) 30 mM Mg^{2+} in the solution.

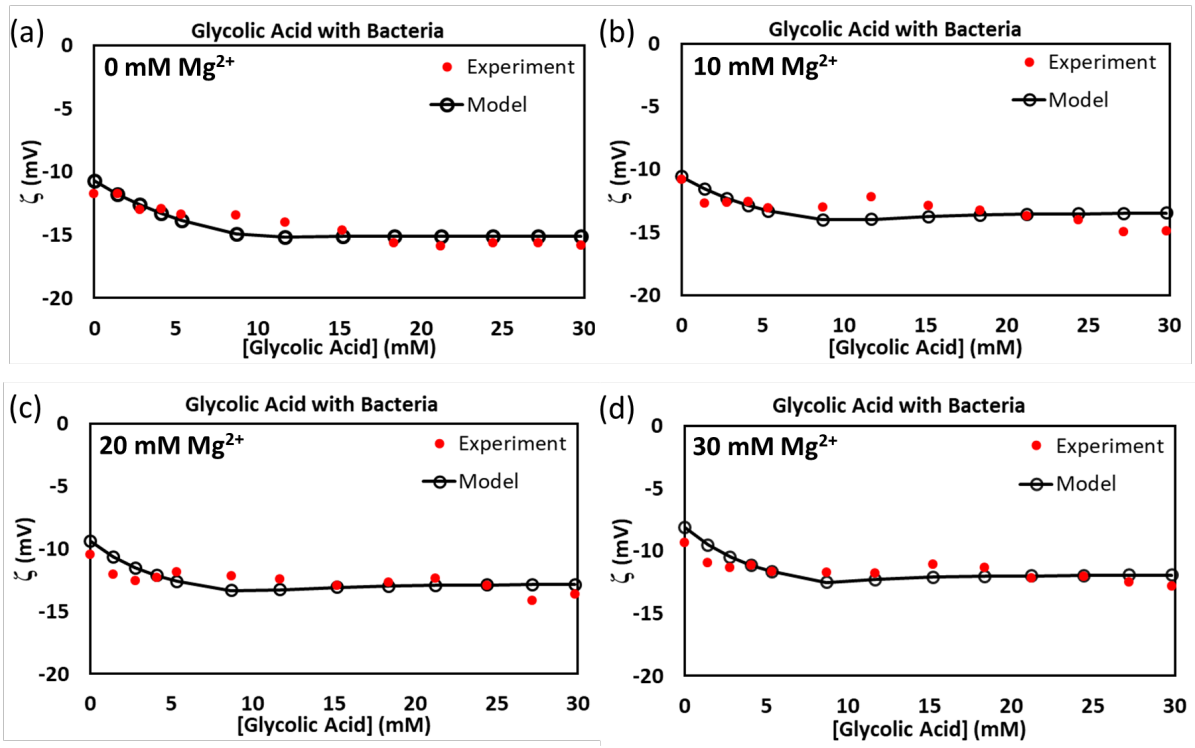

Figure 11. Zeta potential of POA1 as function of different GA concentrations and (a) 0 mM, (b) 10 mM, (c) 20 mM and (d) 30 mM Mg^{2+} in the solution.

Table 1. (a) Summary of XPS peaks on both OTEs. (b) Elements ratio on both OTEs determined by XPS.

a)

Peak Label	Binding energy (eV)	Possible functional groups	Surface Coverage BDD/OTE (%)	Surface Coverage OH-BDD/OTE (%)	Reference
C1	284.6 ± 0.15	C-H	41.9	0	[53]
C2	285.1 ± 0.3	C-C	20.8	93.2	[53]
C3	286 ± 0.3	C-O/C=O/ $-(CH_2CH_2NH)_n-$	9.1	4.2	[59]
C4	286.4 ± 0.3	C-OH	18.8	0	[53]
C5	288.7±0.15	-COOH	0	2.6	[53]
C6	285.5	C-NH	9.3	0	[60]

b)

Elements ratio on both OTEs.	BDD/OTE	OH-BDD/OTE
C/O	5.9	4.1
C/N	59.5	17.2
C/Si	64.5	17.4

Table 2. Deprotonation rate constants, their corresponding site numbers, and number of adsorption sites for chelation for EDTA and GA.[§]

	Deprotonation Rate Constant					**Site number (number/nm^2)** [¶]					
Solution	pK_{a1}	pK_{a2}	pK_{a3}	pK_{a4}	K_M	N_{a1}	N_{a2}	N_{a3}	N_{a4}	N_d	ΔG^*
Experimental Solution Condition	3.9 (0.05)	7.4 (0.31)	8.6 (0.67)	10.6 (0.24)	-	6.5 (2.7)	5.4 (1.5)	8.3 (5.4)	16.1 (3.7)	-	-
EDTA, 0 mM	3.3	7.5	5.6	10.3	5.0	11.0	3.3	10.4	15.7	41.	0.4
EDTA, 10 mM	3.3	7.5	5.2	10.3	5.0	11.0	16.3	10.4	15.9	62.	0.4
EDTA, 20 mM	3.3	7.5	5.2	10.3	5.0	11.0	16.3	10.4	15.9	62.	0.4
EDTA, 30 mM	3.3	7.5	5.2	10.3	5.0	11.0	16.3	10.4	15.9	57.	0.4
GA, 0 mM Mg^{2+}	3.3	7.5	6.4	10.3	5.0	2.8	16.3	10.4	16.0	44.	5.0
GA, 10 mM Mg^{2+}	3.3	7.5	6.2	10.3	5.0	8.9	16.3	10.4	16.0	50.	5.0
GA, 20 mM Mg^{2+}	3.3	7.5	5.9	10.3	5.0	11.0	16.3	10.4	16.0	66.	5.0
GA, 30 mM Mg^{2+}	3.3	7.5	5.2	10.3	5.0	11.0	16.3	10.4	16.0	76.	5.0

[§]Standard deviation for experimental values is given in parentheses. [*]ΔG is the free energy in kJ/mol. [¶] Site volume number density was converted to surface number density assuming a uniform site distribution along a 50 nm fibril length.[42]

References

1 H. C. Flemming, Biofouling in water systems - Cases, causes and countermeasures, *Appl. Microbiol. Biotechnol.*, 2002, **59**, 629–640.

2 T. Abee, L. Krockel and C. Hill, Bacteriocins: modes of action and potentials in food preservation and control of food poisoning, *Int. J. Food Microbiol.*, 1995, **28**, 169–185.

3 P. E. Granum, J. M. Tomas and J. E. Alouf, A survey of bacterial toxins involved in food poisoning: a suggestion for bacterial food poisoning toxin nomenclature, *Int. J. Food Microbiol.*, 1995, **28**, 129–144.

4 Y. H. An and R. J. Friedman, Concise review of mechanisms of bacterial adhesion to biomaterial surfaces, *J. Biomed. Mater. Res.*, 1998, **43**, 338–348.

5 A. J. van der Borden, H. van der Werf, H. C. van der Mei and H. J. Busscher, Electric-current-induced detachment of Staphylococcus epidermidis strains from surgical stainless steel., *J. Biomed. Mater. Res. B. Appl. Biomater.*, 2004, **68**, 160–164.

6 M. Cloutier, D. Mantovani and F. Rosei, Antibacterial Coatings: Challenges, Perspectives, and Opportunities, *Trends Biotechnol.*, 2015, **33**, 637–652.

7 T. R. Garrett, M. Bhakoo and Z. Zhang, Bacterial adhesion and biofilms on surfaces, *Prog. Nat. Sci.*, 2008, **18**, 1049–1056.

8 C. Liu, X. Xie, W. Zhao, N. Liu, P. A. Maraccini, L. M. Sassoubre, A. B. Boehm and Y. Cui, Conducting Nanosponge Electroporation for Affordable and High-Efficiency Disinfection of Bacteria and Viruses in Water, *Nano Lett.*, 2013, **13**, 4288–4293.

9 Q. Zhang, J. Nghiem, G. J. Silverberg and C. D. Vecitis, Semiquantitative performance and mechanism evaluation of carbon nanomaterials as cathode coatings for microbial fouling reduction, *Appl. Environ. Microbiol.*, 2005, **81**, 4744–4755.

10 I. Gall, M. Herzberg and Y. Oren, The effect of electric fields on bacterial attachment

to conductive surfaces, *Soft Matter*, 2013, **9**, 2443–2452.

11 J. P. Busalmen, S. R. De Sánchez and S. R. De Sa, Electrochemical polarization-induced changes in the growth of individual cells and biofilms of Pseudomonas fluorescens (ATCC 17552), *Appl. Environ. Microbiol.*, 2005, **71**, 6235–6240.

12 A. Ronen, W. Duan, I. Wheeldon, S. Walker and D. Jassby, Microbial attachment inhibition through low-voltage electrochemical reactions on electrically conducting membranes, *Environ. Sci. Technol.*, 2015, **49**, 12741–12750.

13 S. Pandit, S. Shanbhag, M. Mauter, Y. Oren and M. Herzberg, The influence of electric fields on biofouling of carbonaceous electrodes, *Environ. Sci. Technol.*, 2017, **51**, 10022–10030.

14 C. D. Vecitis, M. H. Schnoor, M. Saifur Rahaman, J. D. Schiffman and M. Elimelech, Electrochemical multiwalled carbon nanotube filter for viral and bacterial removal and inactivation, *Environ. Sci. Technol*, 2011, **45**, 3672–3679.

15 C. A. Martínez-Huitle and E. Brillas, Electrochemical alternatives for drinking water disinfection, *Angew. Chemie - Int. Ed.*, 2008, **47**, 1998–2005.

16 D. He, C. E. Wong, W. Tang, P. Kovalsky and T. D. Waite, Faradaic reactions in water desalination by batch-mode capacitive deionization, *Environ. Sci. Technol Lett.*, 2016, **3**, 222–226.

17 Y. Oren, Capacitive deionization (CDI) for desalination and water treatment — past, present and future (a review), *Desalination*, 2008, **228**, 10–29.

18 M.-H. Lin, S. Mehraeen, G. Cheng, C. Rusinek and B. P. Chaplin, The role of near electrode solution chemistry on bacteria attachment and inactivation at low applied potentials, *Environ. Sci. Technol*, 2020, **54**, 446–455.

19 H.-L. Alakomi, M. Saarela and I. M. Helander, Effect of EDTA on Salmonella enterica serovar Typhimurium involves a component not assignable to

lipopolysaccharide release, *Microbiology*, 2003, **149**, 2015–2021.

20 C. Belfiore, P. Castellano and G. Vignolo, Reduction of Escherichia coli population following treatment with bacteriocins from lactic acid bacteria and chelators, *Food Microbiol.*, 2007, **24**, 223–229.

21 M. A. Asbell and R. G. Eagon, Role of Multivalent Cations in the Organization, Structure, and Assembly of the Cell Wall of Pseudomonas aeruginosa, *J. Bacteriol.*, 1966, **92**, 380–387.

22 H. Mulcahy, L. Charron-Mazenod and S. Lewenza, Extracellular DNA Chelates Cations and Induces Antibiotic Resistance in Pseudomonas aeruginosa Biofilms, *PLoS Pathog.*, 2008, **4**, e1000213 (1-12).

23 K. J. Thomas and C. V. Rice, Revised model of calcium and magnesium binding to the bacterial cell wall, *BioMetals*, 2014, **27**, 1361–1370.

24 E. Banin, K. M. Brady and E. P. Greenberg, Chelator-induced dispersal and killing of Pseudomonas aeruginosa cells in a biofilm., *Appl. Environ. Microbiol.*, 2006, **72**, 2064–2069.

25 S. K. Maier, S. Scherer and M. J. Loessner, Long-chain polyphosphate causes cell lysis and inhibits Bacillus cereus septum formation, which is dependent on divalent cations, *Appl. Environ. Microbiol.*, 1999, **65**, 3942–3949.

26 P. Corbisier, D. Van Der Lelie, B. Borremans, A. Provoost, V. De Lorenzo, N. L. Brown, J. R. Lloyd, J. L. Hobman, E. Csöregi, G. Johansson and B. Mattiasson, Whole cell- and protein-based biosensors for the detection of bioavailable heavy metals in environmental samples, *Anal. Chim. Acta*, 1999, **387**, 235–244.

27 D. J. R. Conroy, P. A. Millner, D. I. Stewart and K. Pollmann, Biosensing for the environment and defence: aqueous uranyl detection using bacterial surface layer proteins, *Sensors*, 2010, **10**, 4739–4755.

28 J. Maly, E. Illiano, M. Sabato, M. De Francesco, V. Pinto, A. Masci, D. Masci, J. Masojidek, M. Sugiura, R. Franconi and R. Pilloton, Immobilisation of engineered molecules on electrodes and optical surfaces, *Mater. Sci. Eng. C*, 2002, **22**, 257–261.

29 A. Loukanov, A. Angelov, Y. Takahashi, I. Nikolov and S. Nakabayashi, Carbon nanodots chelated with metal ions as efficient electrocatalysts for enhancing performance of microbial fuel cell based on sulfate reducing bacteria, *Colloids Surfaces A Physicochem. Eng. Asp.*, 2019, **574**, 52–61.

30 A. Y. Bhagirath, Y. Li, D. Somayajula, M. Dadashi, S. Badr and K. Duan, Cystic fibrosis lung environment and Pseudomonas aeruginosa infection, *BMC Pulm. Med.*, 2016, **16**, 174–190.

31 G. Cheng, Z. Zhang, S. Chen, J. D. Bryers and S. Jiang, Inhibition of bacterial adhesion and biofilm formation on zwitterionic surfaces, *Biomaterials*, 2007, **28**, 4192–4199.

32 P. Gayen and B. P. Chaplin, Fluorination of Boron-Doped Diamond Film Electrodes for Minimization of Perchlorate Formation, *ACS Appl. Mater. Interfaces*, 2017, **9**, 27638–27648.

33 J. R. Wayment and J. M. Harris, Controlling binding site densities on glass surfaces, *Anal. Chem.*, 2006, **78**, 7841–7849.

34 A. Alghunaim, E. T. Brink, E. Y. Newby and B. Zhang Newby, Retention of poly(N-isopropylacrylamide) on 3-aminopropyltriethoxysilane, *Biointerphases*, 2017, **12**, 1–9.

35 A. F. Stalder, G. Kulik, D. Sage, L. Barbieri and P. Hoffmann, A snake-based approach to accurate determination of both contact points and contact angles, *Colloids Surfaces A Physicochem. Eng. Asp.*, 2006, **286**, 92–103.

36 A.-G. Rincón and C. Pulgarin, Effect of pH, inorganic ions, organic matter and H2O2 on E. coli K12 photocatalytic inactivation by TiO2 Implications in solar water

disinfection, *Appl. Catal. B Environ.*, 2004, **51**, 283–302.

37 Y. Hong and D. G. Brown, Alteration of bacterial surface electrostatic potential and pH upon adhesion to a solid surface and impacts to cellular bioenergetics, *Biotechnol. Bioeng.*, 2010, **105**, 965–972.

38 Y. Hong and D. G. Brown, Electrostatic behavior of the charge-regulated bacterial cell surface, *Langmuir*, 2008, **24**, 5003–5009.

39 H. . Frisch, M. J.; Trucks, G. W.; Schlegel, H. B.; Scuseria, G. E.; Robb, M. A.; Cheeseman, J. R.; Scalmani, G.; Barone, V.; Petersson, G. A.; Nakatsuji, *Gaussian 16 Rev. B.01. Wallingford, CT 2016*, .

40 A. V. Marenich, C. J. Cramer and D. G. Truhlar, Universal solvation model based on solute electron density and on a continuum model of the solvent defined by the bulk dielectric constant and atomic surface tensions, *J. Phys. Chem. B*, 2009, **113**, 6378–6396.

41 J. Lyklema, *Fundamentals of interface and colloid science: liquid-fluid interfaces*, Academic Press, 2000.

42 A. Poortinga, R. Bos and W. Norde, Electric double layer interactions in bacterial adhesion to surfaces, *Surf. Sci. Rep.*, 2002, **47**, 3–32.

43 T. W. Healy and L. R. White, Ionizable surface group models of aqueous interfaces, *Adv. Colloid Interface Sci.*, 1978, **9**, 303–345.

44 R. J. Hunter, *Zeta potential in colloid science : principles and applications*, Academic Press, New York, 1981.

45 Y.-I. Chang and C.-Y. Hsieh, The effect of cationic electrolytes on the electrophoretic properties of bacterial cells, *Colloids and Surfaces*, 1991, **53**, 21–31.

46 B. E. Conway, *Transition from 'Supercapacitor' to 'Battery' Behavior in Electrochemical Energy Storage*, 1991, vol. 138.

47 S. Nayak and B. P. Chaplin, Fabrication and characterization of porous, conductive, monolithic Ti 4 O 7 electrodes, *Electrochim. Acta*, 2018, **263**, 299–310.

48 David Nicholls, *Complexes and First-Row Transition Elements*, Macmillan, 1974.

49 A. S. Ambolikar, S. K. Guin and S. Neogy, An insight into the outer- and inner-sphere electrochemistry of oxygenated single-walled carbon nanohorns (o-SWCNHs), *New J. Chem.*, 2019, **43**, 18210–18219.

50 W. Richard, D. Evrard and P. Gros, Kinetic study of redox probes on glassy carbon electrode functionalized by 4-nitrobenzene diazonium, *Int. J. Electrochem. Sci*, 2019, **14**, 453–469.

51 P. Chen and R. L. McCreery, Control of Electron Transfer Kinetics at Glassy Carbon Electrodes by Specific Surface Modification, *Anal. Chem.*, 1996, **68**, 3958–3965.

52 B. P. Chaplin, Critical review of electrochemical advanced oxidation processes for water treatment applications, *Environ. Sci. Process. Impacts*, 2014, **16**, 1182–1203.

53 P. Gayen and B. P. Chaplin, Selective electrochemical detection of ciprofloxacin with a porous nafion/multiwalled carbon nanotube composite film electrode, *ACS Appl. Mater. Interfaces*, 2016, **8**, 1615–1626.

54 Y. Hong and D. G. Brown, Cell surface acid–base properties of Escherichia coli and Bacillus brevis and variation as a function of growth phase, nitrogen source and C:N ratio, *Colloids Surfaces B Biointerfaces*, 2006, **50**, 112–119.

55 N. H. Lam, Z. Ma and B.-Y. Ha, Electrostatic modification of the lipopolysaccharide layer: competing effects of divalent cations and polycationic or polyanionic molecules, *Soft Matter*, 2014, **10**, 7528–7544.

56 A. T. Poortinga, R. Bos and H. J. Busscher, Electrostatic interactions in the adhesion of an ion-penetrable and ion-impenetrable bacterial strain to glass, *Colloids Surfaces B Biointerfaces*, 2001, **20**, 105–117.

57 R. L. Dehaan, The effects of the chelating agent ethylenediamine tetra-acetic acid on cell adhesion in the slime mould Dictyostelium discoideum, *j. Embryol. exp. Morph*, 1959, **7**, 335–343.

58 A. T. Poortinga, R. Bos, W. Norde and H. J. Busscher, Electric double layer interactions in bacterial adhesion to surfaces, *Surf. Sci. Rep.*, 2002, **47**, 1–32.

59 G. Beamson and D. Briggs, *High resolution XPS of organic polymers: The Scienta ESCA 300 database.*, Wiley-Blackwell, 1992, vol. 20.

60 J. S. Lee, D. H. Shin and J. Jang, Electronic Supplementary Information (ESI) for Polypyrrole-coated manganese dioxide with multiscale architectures for ultrahigh capacity energy storage, *Energy Environ. Sci.*, 2015, **8**, 3030–3039.